

Wrapping liquids, solids, and gases in thin sheets

Joseph D. Paulsen¹

¹Department of Physics, Syracuse University, Syracuse, NY 13244 USA; email: jdpaulse@syr.edu

Xxxx. Xxx. Xxx. Xxx. YYYY. AA:1–20

[https://doi.org/10.1146/\(\(please add article doi\)\)](https://doi.org/10.1146/((please add article doi)))

Copyright © YYYY by Annual Reviews.
All rights reserved

Keywords

elastic sheets, isometries, inflated surfaces, buckling, wrinkling, geometric incompatibility

Abstract

Many objects in nature and industry are wrapped in a thin sheet to enhance their chemical, mechanical, or optical properties. There are similarly a variety of methods for wrapping, from pressing a film onto a hard substrate, to using capillary forces to spontaneously wrap droplets, to inflating a closed membrane. Each of these settings raises challenging nonlinear problems involving the geometry and mechanics of a thin sheet, often in the context of resolving a geometric incompatibility between two surfaces. Here we review recent progress in this area, focusing on highly bendable films that are nonetheless hard to stretch, a class of materials that includes polymer films, metal foils, textiles, graphene, as well as some biological materials. Significant attention is paid to two recent advances: (i) a novel isometry that arises in the doubly-asymptotic limit of high flexibility and weak tensile forcing, and (ii) a simple geometric model for predicting the overall shape of an interfacial film while ignoring small-scale wrinkles, crumples, and folds.

1. INTRODUCTION

Many three-dimensional objects are wrapped in two-dimensional sheets to enhance their properties. We wrap gifts to decorate or hide the contents, we wrap foods in plastic, foil, or dough to hold them together or preserve them, and we wrap ourselves up to stay warm or fashionable. We sometimes take advantage of permeability: a paper bag ripens avocados or bananas by holding in gas released by the fruit while letting smaller air molecules through. Under the right conditions, a sheet can even dictate the bulk properties of its contents: coffee grounds poured into a bag become mechanically rigid when a vacuum seal is applied. The general strategy of covering an object with a thin veneer is so pervasive that the file format of this very document contains a layer of code called a wrapper.

Clearly there is a variety of uses for wrappers, which also cover a large range of physical scales. Figure 1 shows examples that span 9 orders of magnitude in size, from graphene nanosacks to super-pressure balloons. Of course, there are other ways to encapsulate an object. A solid surface can be coated using evaporation or chemical reactions, and droplets or bubbles can be covered with surfactants or particles. Nevertheless, a sheet offers a strong barrier without gaps, and can serve as a platform for adding further functionality.

Still, one faces a challenge when trying to cover a ball with wrapping paper — the whole process seems messy and inefficient. What are the geometric constraints encountered when placing a flat sheet around a curved object? What is the area and shape of the smallest wrapper that will suffice? Why is stress sometimes focused at sharp points or ridges, and when can smooth wrappings be achieved? These issues are further complicated

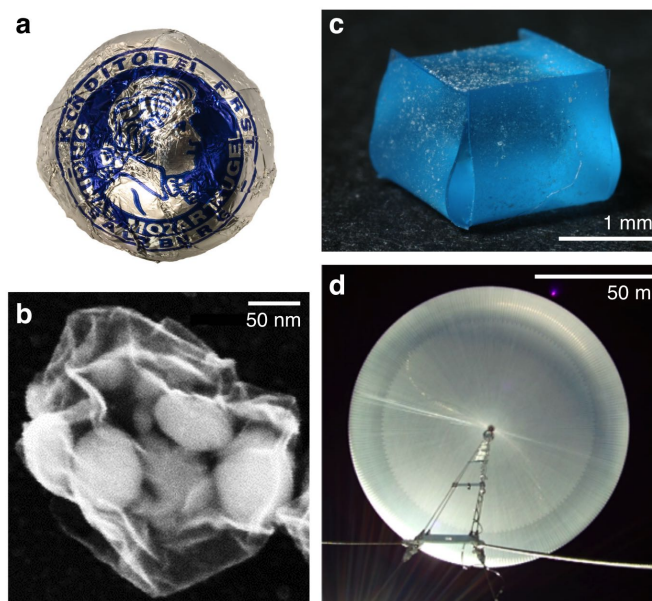


Figure 1

Thin sheet wrappers in a variety of settings. (a) A confection wrapped in metal foil, modeled in Reference 1 (image: Wikimedia Commons). (b) Graphene sacks holding colloidal particles, adapted from Reference 2 with permission. (c) A water droplet wrapped in a PDMS film, adapted from Reference 3 with permission. (d) A scientific balloon at 110,000 feet (image courtesy NASA).

by nonlinearities: a thin sheet can adopt many different conformations, and large curvature or self contact are easy to achieve. Because they are intrinsic to the geometry of the deformations, these nonlinearities apply to any material, even when the local stress-strain relation is linear (i.e., Hookean) (4).

This article discusses recent advances around these questions in a wide variety of contexts spanning basic and applied research in mechanical, chemical, and aerospace engineering, soft matter physics, and mathematics. One fruitful approach has been to divide and conquer, i.e., isolating and studying a specific morphology, one at a time. This reductionist strategy has produced a catalog of buckled microstructures along with their origin. (We describe just a few in Section 3.) A second approach aims to describe the overall response of the film. Recent work has uncovered a surprising limit where a sufficiently thin sheet can hug an arbitrary contour with vanishing strain energy. We describe this so called “asymptotic isometry” in Section 4. These results form the basis for a powerful geometric model for a thin film attached to a liquid surface, described in Section 5. This model uncovers a fundamental connection between ultrathin liquid wrappers and inflated bags, which are the subject of Section 6. We close by discussing some open problems and opportunities.

2. GEOMETRY AND MECHANICS OF THIN ELASTIC SHEETS

2.1. Bending versus stretching

When unrolling plastic wrap, handling a large flimsy poster, or watching a fluttering flag, we become aware of the multitude of deformations that are available to thin materials. We can begin to understand these behaviors by the simple act of rolling a sheet of paper into a tube. Due to the finite thickness of the sheet, t , the outer surface has a circumference that is $\sim t$ longer than inner edge, for any tube radius R . Thus, the material is compressed on its inner face and stretched on its outer face by a strain of $\Delta L/L \sim t/2R$ (ignoring corrections due to the Poisson effect). For loosely-rolled printing paper where the short edges are just brought into contact, the strain on the faces is thus $\sim 0.1\%$, so the material deformations are well within the linear elastic regime (5).

For this case of pure bending, the elastic energy per unit area is B/R^2 , where $B = Et^3/[12(1 - \Lambda^2)]$ is the bending modulus of the sheet, with E the Young’s modulus and Λ the Poisson ratio. The total energy is then ~ 8 mJ, quantifying the small effort required to roll up the sheet. Stretching the sheet with the same total energy would displace the edges by only ~ 200 μm . Comparing the characteristic energy scales for stretching versus bending gives the dimensionless von Kármán number, $W^2Y/B \sim (W/t)^2$ (6) (where $Y = Et$ is the stretching modulus of the sheet and W is a characteristic lateral scale). The appearance of the ratio W/t shows that the relative ease of bending (versus stretching) is a purely geometric phenomenon that applies to any material made sufficiently thin.

2.2. Buckling and wrinkling

Because of this low bending cost, thin sheets tend to buckle under compression. Beyond a critical load, a long-wavelength bending deformation is energetically favored over in-plane compression. The critical load, derived by Leonhard Euler in 1757, is proportional to Et^3/L^2 and is thus vanishingly small for thin films (7). This fact exemplifies a broader qualitative result: a thin sheet favors *isometric deformations*, i.e., those that preserve distances as measured along the sheet.

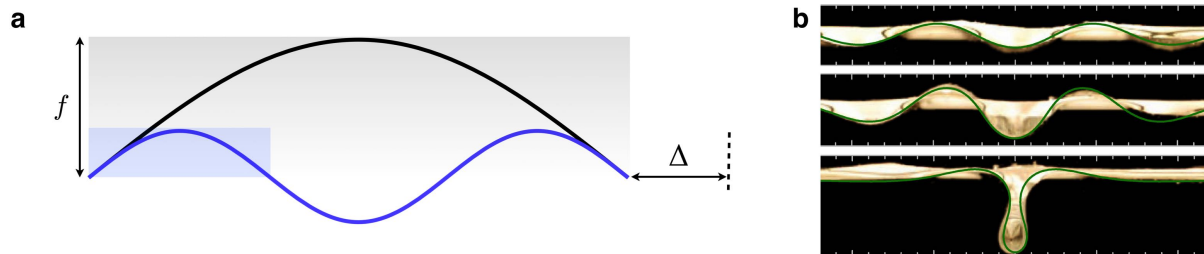


Figure 2

Bending and wrinkling of slender objects. (a) Black line: idealized sinusoidal buckling of a sheet due to compression by a distance Δ . The arclength of this curve is unchanged if it is scaled down by a factor of n and repeated n times ($n = 3$ for the blue curve). (b) Wrinkle-to-fold transition in a polyester film floating on water. The sequence of images shows the response to increasing compression from the edges (8). Green lines: exact analytic solution with no free parameters (9). Adapted from Reference 10 with permission.

The formation of smooth parallel wrinkles is a conceptually similar isometry, and the wrinkle wavelength affords an insight into the mechanics of the sheet and the substrate. Consider a sheet floating on a liquid bath that is laterally compressed by a fixed amount Δ . Buckling into a single arch or valley displaces a large volume of liquid under the sheet. This gravitational cost may be reduced by creating multiple undulations of amplitude f and wavelength λ — fixing the ratio f/λ keeps the total compression unchanged (see Fig. 2a). Integrating the arclength of a small-amplitude sinusoid yields a simple relationship between the wrinkle amplitude, wavelength, and fractional compression $\tilde{\Delta} \equiv \Delta/L$, namely:

$$\frac{f}{\lambda} \approx \frac{\sqrt{\tilde{\Delta}}}{\pi}. \quad 1.$$

This result is called the “slaving condition” (11).

Although they are beneficial for the substrate, smaller wavelength wrinkles pose a larger bending cost. Minimizing the sum of the sheet and substrate energies gives a simple law for the preferred wavelength, $\lambda = 2\pi(B/\rho g)^{1/4}$, which agrees with experiments (8, 12). Remarkably, this relation may be generalized to include the restoring force of a liquid or elastic substrate (13, 14), tension along the direction of the wrinkle crests (15), and curvature along the wrinkles (16, 17), even in nonuniform curved topographies. In particular,

$$\lambda = 2\pi(B/K_{\text{eff}})^{1/4}, \quad 2.$$

where K_{eff} is an effective substrate stiffness. This “local λ law” (16) offers an inexpensive and non-invasive metrology of thin materials: by measuring the wavelength of a wrinkle pattern, one can infer the mechanical properties of the sheet or the substrate (18, 19). The rational design of wrinkled morphologies enables a variety of practical applications, from sieving particles (20) to tuning wetting and adhesion on a surface (21, 22, 23).

More broadly, the ubiquity of small-scale wrinkles may be attributed to their solving of a general problem: they draw material points towards each other in three-dimensional space with minimal deflection out of plane, all with a low elastic energy cost. This observation is a key conceptual building block for the “asymptotic isometry” described in Section 4.

2.3. Geometric nonlinearities

So far we have limited our discussion to settings where the film may deform isometrically so that in-plane strains are vanishing. Because they automatically minimize the stretching energy, isometries are often a good place to start searching for solutions to a given problem. However, there may be many isometries available, and they may be difficult to parameterize, since slender materials can attain large curvatures and self-contact under moderate forcing. These difficulties fall under the category of “geometric nonlinearities”, as opposed to nonlinearities in the local stress-strain relationship of the material itself. In other words, these geometric issues plague even the simplest Hookean regime of the local material response. (The good news is, an understanding of these effects may be applied to any material.)

Consider the large-scale deflection of a thin rod with a heavy weight at one end: the equation governing this shape is nonlinear due to large rotations. This problem was posed by James Bernoulli in 1691, and similar problems were studied by Galileo, the Bernoullis, Euler, and much later by Max Born (among others) (24). The solutions are called “elastica”, which may be found by extremizing the bending energy (with an inextensibility constraint).

When there are additional energies or more complicated boundary conditions (25), the behaviors are even richer (26, 25). One remarkable example of an exactly solvable problem is a uniaxially-compressed floating film (8, 27, 10, 28). Figure 2b shows the side-view of a floating rectangular polyester film that is compressed from two sides. As the compression increases, the experiment shows a progression from a weakly-buckled sinusoid to a single localized fold. The entire evolution of this system may be described by minimizing the sum of the bending energy of the sheet and the gravitational energy of the liquid (9, 29).

3. GEOMETRIC INCOMPATIBILITY

The problem of wrapping a sphere with a flat sheet (illustrated in Fig. 3a) is a familiar frustration. Flat bandages don’t stick as well to curved knuckles or elbows, and maps of the earth exaggerate areas near the poles. These everyday examples just scrape the surface of all the natural and technological settings where incompatible curvatures arise, from the stamping or forging of automotive metal to the delicate undulating edge of a flower (30).

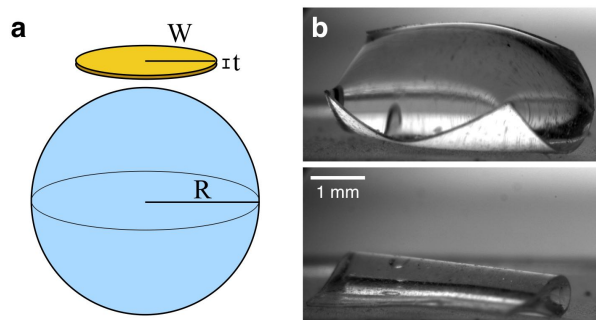


Figure 3

Geometric incompatibility. (a) A planar sheet cannot be mapped onto a doubly curved surface (here a sphere of radius R) without straining the sheet or deforming the surface. (b) Spontaneous wrapping of a water droplet by a square PDMS film. The droplet and sheet deform in a way that preserves distances along the sheet. Adapted from Reference 31 with permission.

Compared to the relative ease with which a flat sheet is isometrically rolled into a tube, one gets the feeling that there are no isometries that take a flat sheet to a sphere, or a spherical cap. This feeling is correct. To categorize the local geometry of an arbitrary surface, Karl Friedrich Gauss defined the “Gaussian curvature” \mathcal{K} as the product of the two principal curvatures at any given point. Under this definition, a cylinder is flat ($\mathcal{K} = 0$), since at every point there is a straight path along the surface (with zero curvature in that direction). The top of a hill or the bottom of a valley have two principal curvatures of the same sign (i.e., both positive or both negative) so $\mathcal{K} > 0$, whereas an equestrian saddle curves upwards along its length and downwards along its width, so $\mathcal{K} < 0$. In his *Theorema Egregium* (“remarkable theorem”, 1828), Gauss proved that local isometries always preserve the Gaussian curvature of the surface (32). Thus, the problem encountered in Fig. 3a is unavoidable: a planar sheet cannot be mapped onto a sphere or saddle without straining the material. Here we take a tour of several qualitatively different resolutions.

3.1. Deforming the wrapped object

Figure 3b shows a square polymer film ($t \sim 60 \mu\text{m}$) resting on a table, with a water droplet of surface tension $\gamma = 72 \text{ mN/m}$ placed on top of it (31). The surface tension of the air-water interface spontaneously curls the edges of the film around the droplet. As the water evaporates, two opposite ends of the wrapper come together. This so-called “capillary origami” is a model example of elastocapillarity, defined broadly as the competition of elastic energies of a solid with surface energies (of the solid itself or a contacting liquid). Other examples include the clumping of wet hair (33) and the blunting of corners on a soft solid (34, 35). For recent reviews of the field, see Refs. (36, 37).

Bending a sheet around a droplet of radius R requires an elastic cost per unit area of B/R^2 , while reducing the surface energy by an amount of order γ per unit area. Equating these expressions gives a so-called bendo-capillary length,

$$\ell_B = \sqrt{B/\gamma}, \quad 3.$$

indicating that this energy “trade” is beneficial for radii of curvature larger than ℓ_B (regardless of the size of the sheet, W). Notably, ℓ_B goes to zero with the sheet thickness as $t^{3/2}$, so that sufficiently thin structures are always prone to deformation by liquid interfaces. Hence, capillary origami offers a method for fabricating three-dimensional objects on small scales where surface forces dominate bulk forces (38).

3.2. Joining flat petals together

The droplet in Fig. 3b is significantly deformed by the square sheet. By choosing a different two-dimensional shape for the wrapper, is it possible to form a closed shape that resembles a sphere? Imagine slicing the surface of a globe along lines of longitude. Peeling these strips off from the north pole while keeping them joined together at a single point at the south pole, one gets a flower-shaped net that lays nearly flat. (The narrower and more numerous the strips, the flatter the unfurled net.) This strategy was used for wrapping thin silicon sheets around water droplets to form three-dimensional solar cells (41). Other shapes can be formed as well; Figure 4a shows an “elastocapillary pipette” that grabs a droplet of specified volume when it is lifted from a pool of liquid (42, 39).

Figure 4b shows a qualitatively different set of three planar strips that form an approximate sphere when they are sewn together (40). Here the petals are not convex. What

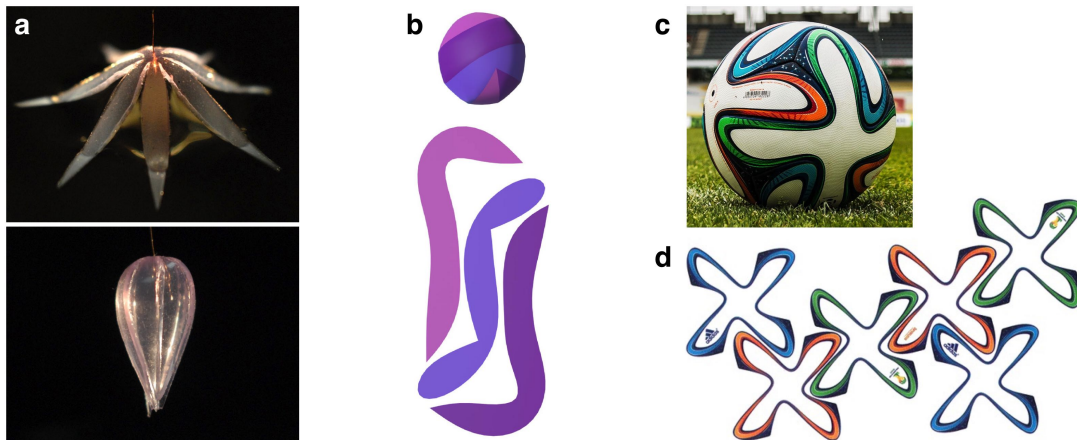


Figure 4

Assembling flat petals into closed surfaces. (a) Elastocapillary pipette formed by a planar polymer film cut into a flower shape (39). As the sheet is lifted, it grabs a droplet from a flat liquid bath. Reproduced with permission from J. Hure (PMMH-ESPCI and MIT). (b) Three flat strips that form an approximately spherical enclosure when they are joined at their edges and inflated. Adapted from Reference 40 with permission. (c) “Brazuca” soccer ball from the 2014 FIFA World Cup. (d) The ball is covered by six identical flat panels (image: Yannick Plissier, Wikimedia Commons).

are the geometric rules that govern the joining of planar sheets along their boundaries? If you start “zipping” two surfaces together, can you always continue in one direction, or will you ever get stuck? Pogorelov answered these questions in the 1970s (43). Remarkably, if the *sum* of the planar curvatures of the panels is positive at every point along the seams, you will always end up with a convex three-dimensional shape with developable faces. (An additional condition is required at corners where the total angle should not exceed 360° .)

These geometric rules have cropped up in the soccer ball used in the 2014 FIFA World Cup in Brazil, shown in Fig. 4c, along with its planar net consisting of six identical panels. As noted by Ghys (44), the assembly has 6 faces, 12 curved edges, and 8 vertices: it is a cube masquerading as a sphere! As before, the panels are designed to minimize stretching in the final shape. In addition to geometric novelty, there are physical consequences to the design: the panel shape affects the aerodynamic drag at different speeds (45).

3.3. Stretching the sheet

The deformations considered so far are approximately isometric; they avoid stretching by curling in only one direction at any given location. The situation in Fig. 5a shows a distinct behavior where small but finite stretching of the sheet is apparent. In experiments by Hure et al. (46), a thin polypropylene film placed on a solid sphere coated in ethanol was found to make contact in a branched structure of meandering paths. Here the fluid plays two roles: it provides the adhesion force that pulls portions of the sheet onto the sphere, and it helps visualize the edges of these contact regions by its dyed blue color.

The emergent pattern is visually arresting and prompts a number of questions. Why does the sheet contact the sphere along zig-zagging paths, and why do these paths branch? Yet, one simple observation — the existence of a characteristic width of the contact regions — is already illuminating. This lengthscale can be understood by considering a region

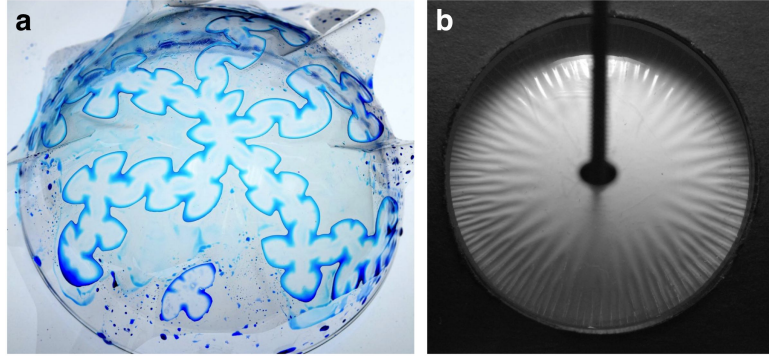


Figure 5

Geometric incompatibility of a thin planar sheet and a hard sphere. (a) Top view of a plastic sheet on a hemisphere coated with ethanol. The thin blue lines are the liquid meniscus at the boundary of the region where the sheet contacts the sphere. Reproduced with permission from J. Hure, J. Bico, and B. Roman (PMMH-ESPCI). (b) A flat circular sheet sandwiched in a thin gap between two spherical caps. As the top (transparent) cap is pushed onto the sheet, a cascade of radial wrinkles emerges. Adapted from Reference 47 with permission.

of radius a where the sheet is stretched onto the sphere of radius R (37). Balancing the reduction in surface energy due to this contact ($\sim \gamma a^2$) with the elastic energy to stretch this patch ($\sim Y a^6 / R^4$), the patch width is estimated to be: $a \sim R(\gamma/Y)^{1/4}$ (48). This scaling is in good agreement with experiments (46). Remarkably, the same lengthscale sets the width of the contact regions in more complex morphologies, obtained at larger R/ℓ_B (46, 49).

Naturally, the more compliant the object, the more it may be stretched by a liquid interface (50, 51, 52, 53). The dimensionless ratio γ/Y gives an estimate of the in-plane strain (37). In general, comparing this value with other (possibly small) strains dictated by geometry or boundary conditions can suggest whether stretching plays a major role (54).

3.4. Wrinkling around a hard sphere

The same model experiment shows another behavior: the sheet delaminates from the sphere over large areas between the adhered regions. What happens if the sheet is forced to follow the shape of the substrate, at least approximately? This occurs when stamping or embossing a flat sheet between two curved plates (55). Figure 5b shows a circular plate of radius W sandwiched between two spherical caps of radius R , studied in Reference 47. When the gap between the plates, δ , is small, a complex and beautiful pattern of wrinkles emerges.

In contrast to the wrinkling of a stiff sheet on a soft substrate considered in Section 2.2, here the wrinkle amplitude is fixed by a hard constraint, i.e., the vertical gap size δ . For a gap of size $\delta \gg t$, the wavelength for wrinkles is set by a simple application of Eqn. 1 with $f = \delta/2$, so that $\lambda \propto \delta$ (for fixed lateral confinement Δ).

The general problem of using wrinkles or other microstructures to accommodate a mismatch in curvature has been considered in a number of settings, from planar sheets on spheres (56) and saddles (57, 16), to curved sheets on flat interfaces (58). Scaling arguments like the ones above can identify key energy and length scales. Sophisticated mathematical treatments have also been developed to establish precise bounds on the ground state energy (59), starting from general theoretical models with minimal assumptions (54, 60).

4. ASYMPTOTIC ISOMETRY

We have just seen that a planar sheet can approximate a spherical cap by forming energetically-cheap wrinkles. These wrinkles allow material points to be drawn towards each other in three-dimensional space with nearly vanishing strain. In the limit of zero thickness, this effective shortening is accomplished with vanishing vertical deflection, which can be seen by considering Eq. 2 along with the slaving condition: $f \propto \lambda$ for fixed compression, Eq. 1. At the same time, when measuring distances along the sheet (traveling up and down the vertical undulations), the original metric of the sheet is barely changed. Thus, the experiment suggests a novel type of isometry that maps a planar sheet arbitrarily close to sphere. We note that such a configuration would not violate Gauss's *Theorema Egregium*: the sheet is nearly unstrained and the metric of the sheet is barely changed.

But the devil is in the details. Does the strain truly vanish in limit of zero thickness, or are there unavoidable regions of stretching associated with some anatomy of the wrinkle pattern? As we will describe next, such an *asymptotic isometry* is indeed possible, which will be borne out in the indentation of a floating ultrathin polymer film. This theoretical approach was developed in a recent sequence of papers (60, 61, 62, 63) that addressed various scenarios in which Gaussian curvature is imposed on a thin sheet (or shell) in the presence of a weak tensile load. In the following, we focus on one example: the indentation of a thin planar sheet that is floating on a flat liquid bath.

4.1. Indenting a floating thin film

From pressing on a peach with your thumb to pushing on graphene with an AFM tip (64), indentation is a ubiquitous and intuitive way to characterize mechanical properties (65). This basic assay has been applied over a wide range of scales, from nanoscale viruses (66) to polymer capsules (67) to macroscopic model ellipsoids (68, 69). Here we describe how a non-trivial class of isometries can arise from this simple act.

Consider a circular thin film of radius W and thickness t floating on a flat liquid bath. The liquid surface tension, γ , pulls at the boundaries, creating a uniform isotropic stress in the film. Indenting the center of the film by an infinitesimal amount simply probes this tension (61). Hence for small vertical displacements, δ , the film behaves like a linear spring: $F = k\delta$, with an effective spring constant $k \approx \gamma$.

For larger displacements, a pattern of wrinkles appears as the boundary of the sheet is drawn radially inwards, shown in Fig. 6a. This state has higher energy than the flat state, as the indenter has performed work, $W = \int_0^\delta F(z)dz$, on the liquid and the film. Displacing liquid under the sheet costs a gravitational potential energy U_{grav} while inward retraction of the edge contributes a cost $U_{\text{surf}} = \gamma(\Delta A_{\text{free}})$, where ΔA_{free} is the additional exposed surface area of the bath. In the sheet, elastic energy is stored in stretching and bending terms, U_{stretch} and U_{bend} . Remarkably, an analysis of the small-slope Föppl-von Kármán equations shows that for a sufficiently thin film, nearly all the work is transmitted to the fluid — only a negligible portion goes to bending and stretching the film (61, 71). The mechanical signature of this behavior is a force on the indenter that is predicted to be:

$$F \approx 4.581(\gamma W)^{2/3}(\rho g)^{1/3}\delta, \quad 4.$$

where the mechanical properties of the film (i.e., bending and stretching moduli) do not appear. We emphasize that this “pseudo-linear” response is attained at finite amplitude, and does not reflect the standard linear response, $F \sim \delta$, for infinitesimal displacement.

This theoretical picture has been supported by experiments. Measurements by Holmes & Crosby (72) show a linear force response with a slope that is independent of film thickness, for PS films with $91 < t < 1140$ nm. The dependence of the force on other parameters was verified with experiments and simulations by Ripp et al. (73). The onset of wrinkling and the extent of the unwrinkled central region, measured by Vella et al. (61), also agree with predictions. Finally, measurements of the vertical profile by Paulsen et al. (16) follow the theoretically-predicted shape, shown in Fig. 6b. The lateral scale of a *liquid* meniscus is given by the capillary-gravity length, $\ell_c = \sqrt{\gamma/\rho g}$. In the case of a sheet, the profile is wider by a factor of $(W/\ell_c)^{1/3}$. Hence, the finite size of the sheet is always relevant.

The transmission of a negligible fraction of the work to the sheet reflects a remarkable geometric property: the wrinkled film is nearly isometric to its pre-indentation state. This *asymptotic isometry* is a non-trivial consequence of two simultaneous limits: small bending modulus, $B \ll \gamma W^2$, and small applied tension, $\gamma \ll Y$. Simply taking the limit of zero thickness would achieve the first inequality, but not the second, as the sheet would be significantly stretched by surface tension when $t \lesssim \gamma/E$ (53, 37). In this doubly-asymptotic limit, strains in the film are vanishing everywhere: azimuthal compression is relaxed by the

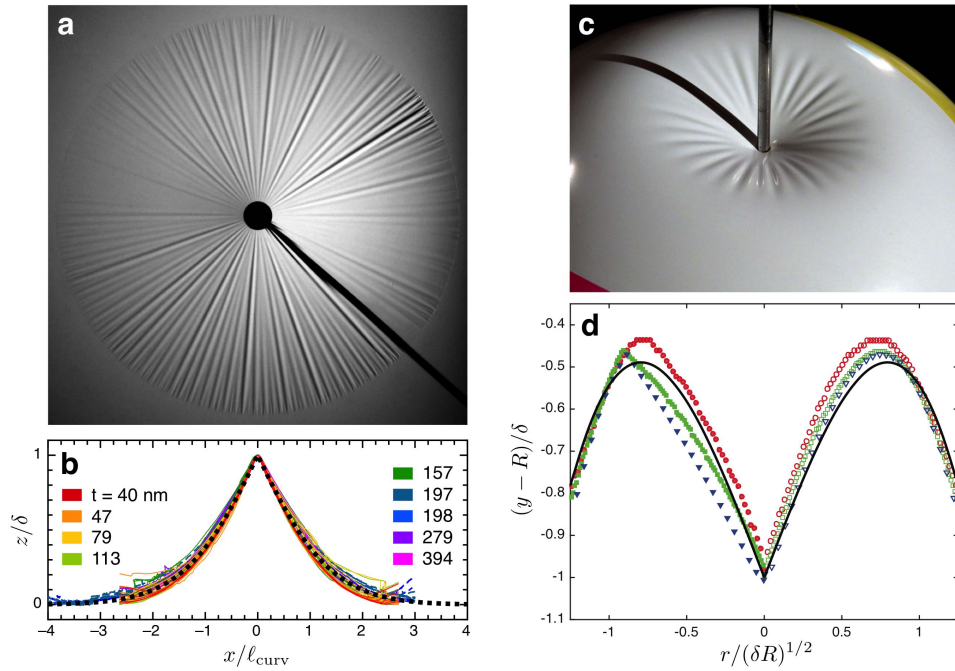


Figure 6

Asymptotic isometry in indentation. (a) Top view of a floating circular polymer film that is poked by a spherical ball bearing from below. (b) Vertical profile of the sheet scaled by the displacement at the center, δ , versus the x -coordinate scaled by $\ell_{\text{curv}} = (W\gamma/\rho g)^{1/3}$. Dashed line: asymptotic isometry prediction with no free parameters (16). (c) Wrinkling of an indented beach ball. (d) Scaled height versus radial coordinate in numerical simulations of an inflated spherical shell. Closed symbols: wrinkle troughs. Open symbols: wrinkle crests. Solid line: asymptotic isometry prediction. Panels (b-d) adapted with permission from References 16, 70, and 63, respectively.

formation of small-scale wrinkles, and radial stretching becomes negligible (61). This result highlights the extreme flexibility of a thin film, which can approximate a doubly-curved surface arbitrarily well with vanishing strain.

4.2. Pressurized shells, twisted ribbons, and beyond

Vella et al. (63) recently demonstrated a similar response in the indentation of a pressurized shell. In a well-known isometry called “mirror buckling”, a portion of the shell is inverted into a concave spherical cap that is a mirror reflection of its original shape (74). But a poked beach ball doesn’t mirror-buckle, it wrinkles, like the one in Fig. 6c. Theoretical calculations find a wrinkled isometry that agrees with finite-element simulations (63). As with the indented floating film (Eq. 4), only a negligible fraction of the work is done on the sheet — nearly all the work is done on the gas. Here the doubly-asymptotic limit is of vanishing thickness and pressure, requiring the gas pressure to vanish as t^α with $1 < \alpha < 2$ (63). If the pressure is any smaller, bending energies are expected to dominate and yet other morphologies may arise (75, 76).

The above studies are all in axially-symmetric geometries. Still more asymptotic isometries arise when a long rectangular sheet is held at its ends and twisted. By controlling the amount of tension and twist, a surprisingly rich set of states may be observed (77, 78). The ribbon can form wrinkles in a region around its centerline, generate flat triangular facets connected by sharp ridges (79, 80), or follow a simple helocoid. Chopin et al. (62) demonstrated that each of these states can be constructed with vanishing strain.

Here we have discussed a new class of isometries that are qualitatively different from those in sheets with unconstrained boundaries (81, 82, 83, 84, 85). The general ingredients for these behaviors appear to be the weak tensile forcing of a thin film. The modesty of these requirements suggests that even more asymptotic isometries await discovery.

5. WRAPPING DROPLETS IN ULTRATHIN SHEETS

We now consider the wrapping of a water droplet by an ultrathin polymer film, a scenario studied recently by Paulsen et al. (86), building on earlier experiments by King et al. (56). This process is partly underway in Fig. 7a, where a $t = 39$ nm polystyrene film sits atop a water droplet surrounded by oil. In contrast to the capillary origami of Fig. 3b, here the bending rigidity of the film is vanishingly small: $B/\gamma W^2 \sim 10^{-7}$ in this instance. Thus, one might expect that the extremely floppy sheet would form a wrinkled envelope in the shape of a sphere. Surprisingly, the symmetry is markedly broken for smaller droplets: the sheet deforms the drop into a triangular shape, shown in Fig. 7b. The same overall shape is formed by a sheet that is 10 times thicker (Fig. 7c). This observation signals a behavior that is governed by geometry rather than a competition of energies.

5.1. Geometric model

To account for these observations, Paulsen et al. (86) introduced a simple geometric model. As in the asymptotic isometries described in Sec. 4, the bending energies are negligible, and vanishing in-plane strains may be captured by imposing an inextensibility constraint on the sheet. The only remaining cost is the surface energy:

$$U = \gamma A_{\text{free}}, \tag{5}$$

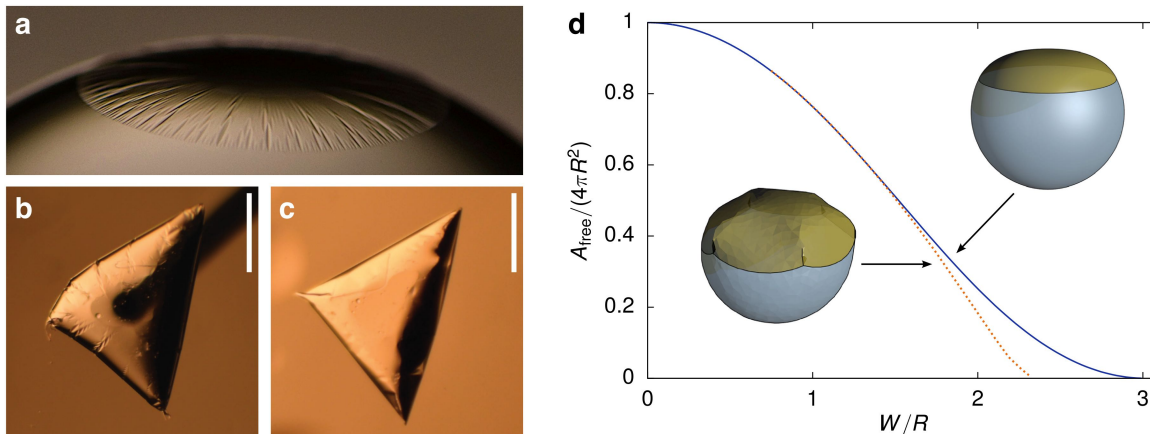


Figure 7

Optimal wrapping with ultrathin sheets (86). (a) A circular polystyrene sheet of thickness $t = 39$ nm and radius $W = 1.5$ mm on a large water droplet in oil. (b) A circular sheet of thickness $t = 29$ nm deforms a small droplet into a triangular shape. (c) The same overall shape occurs for a circular $t = 241$ nm sheet. Scale bar: 1 mm. (d) Normalized exposed interfacial area, $A_{\text{free}}/(4\pi R^2)$, versus the ratio W/R , where R is the radius of a spherical droplet with the same volume. Smaller A_{free} is energetically favored for any W/R . Solid line: optimal axisymmetric wrapping. Dashed line: results from numerical simulations, which find lower-energy states for small droplets (large W/R). Adapted from Reference 86.

where A_{free} is the area of the exposed oil-water interface. Thus, the model favors three-dimensional configurations that minimize A_{free} . (The surface area of the sheet is approximately constant under wrinkling deformations, so the sheet-liquid surface energies may be ignored.) Within this model, the authors focused on the gross shape of the sheet, which ignores the small-scale structure of wrinkles or other buckled morphologies. In the gross shape, material points may move closer to each other (through long-wavelength bending or buckled microstructures), but not farther away, since this would require stretching.

In the case of a large droplet, the model can be solved exactly by assuming an axially-symmetric gross shape for the sheet. The solution is a family of curves where a spherical droplet is joined onto an elliptic integral, in good agreement with experiments (86). At small droplet volumes, more efficient wrappers can be found with broken axial symmetry. Finite-element numerical simulations of Eq. 5 in Surface Evolver (87) have produced such states; one is shown in Fig. 7d. Thus, the triangular wrappings shown in Fig. 7 arise out of a geometric optimization: they are highly efficient containers for a liquid parcel. (An even more efficient empanada shape is obtained in some of the experiments. There may be a finite energy barrier between this state and the triangular wrapping.)

The success of this geometric model has several important consequences. First, these wrappings are optimally efficient: because the energy is proportional to the unwrapped area, the sheets automatically find overall shapes with maximal coverage. Furthermore, they accomplish this in the asymptotic limit of zero thickness, so the amount of raw material needed for the films is minimized. This is precisely what one may desire for an application.

Second, the tendency to wrap is independent of the surface properties of the sheet. This result has been demonstrated dramatically by the spontaneous wrapping of a water droplet in a thin teflon film by Gao & McCarthy (88). Thus, an ultrathin film provides a robust platform for adding chemical patterning and further functionality to liquid droplets, since

the wrapped shapes will not depend on the surface properties of the film.

Third, this model demonstrates a powerful approach for predicting the overall shape of an extremely bendable film in a curved geometry. In general, one has to deal with the highly-nonlinear Föppl–von Kármán equations, which are used to minimize an elastic energy $U_{\text{bend}} + U_{\text{stretch}}$ without any preliminary assumptions. Here, a simple geometric optimization (i.e., a minimization of an area) was used to sidestep these equations entirely.

5.2. Geometry-driven folding

Perhaps even more subtle and surprising is the appearance of folds from a purely geometric mechanism. Microstructural transitions (such as the wrinkle-to-fold transition in 1D) are typically driven by an energetic competition between substrate deformation and bending resistance, so that the phenomenon depends strongly on sheet thickness (89, 90, 91, 92, 10). When wrapping with a sufficiently thin film, folding is instead governed purely by geometry.

A similar geometrically-driven folding transition can be demonstrated in even a simple planar experimental setup, first investigated by Pineirua et al. (93). When a floating annular-shaped film is subjected to a sufficiently large tension on its inner boundary compared to the tension on its outer boundary (controlled by an insoluble surfactant), static forces fall out of balance and the sheet must contract radially inwards. Paulsen et al. (94) showed that for a sufficiently thin film, folding occurs at a threshold ratio of inner to outer tension that depends only on a single geometric parameter, namely, the ratio of the inner to the outer radius. Furthermore, they showed that by changing the size of the hole in the sheet, the collapse can either be continuous or discontinuous.

5.3. Solid surfactants

More broadly, this work opens up possibilities for using elastic sheets to tailor their mechanical, chemical, or optical properties of droplets and liquid interfaces (86, 95). In analogy with molecular or particulate surfactants (96, 97, 98), a thin sheet may act as a “solid surfactant”, which can endow a liquid interface with distinct mechanical responses.

The design space is large: sheets can be cut into different planar shapes, they can be single layers or bilayers with different chemistries on opposite faces (95), they may be flat or curved (58), and so on. Furthermore, existing technologies such as roll-to-roll processing and lithography can be harnessed for cheap mass production. But first, there is fundamental science to do. The mechanical properties of wrapped droplets are just now being uncovered (86) — countless problems dealing with statics and dynamics of sheet-laden droplets and interfaces await exploration.

6. WRAPPING AIR: INFLATING AN INEXTENSIBLE MEMBRANE

6.1. A circular mylar balloon

Another type of wrapping occurs when inflating a bag. Consider a common party balloon that is formed by sealing together the edges of two flat discs of Mylar, a stiff polymer film that is often coated in a reflective layer of aluminum. When filled with gas, the bag inflates to a characteristic shape that looks somewhat ellipsoidal. What is the volume of this shape? What is the shape itself, i.e., the height function $f(r)$ along a meridian? What are the relevant mechanics leading to this equilibrium form? Closer inspection shows that the

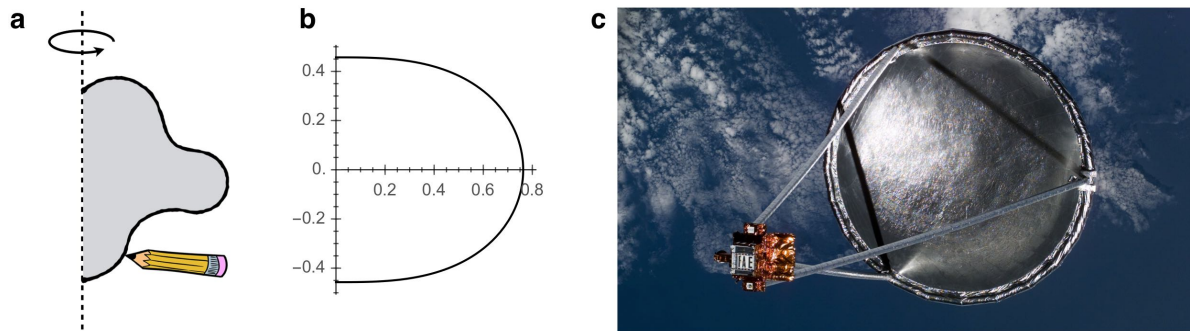


Figure 8

Inflated surfaces. (a) A surface of revolution formed by spinning a curve around an axis. (b) The circular mylar balloon shape, Eq. 6. (c) Inflatable antenna launched from Space Shuttle Endeavour in 1996 (courtesy NASA).

surface is decorated by a multitude of radial wrinkles, as well as sharp crumpled structures. Is it important to understand the microstructures in detail to explain the gross shape?

W. H. Paulsen (99) modeled this problem by noting that inflating the balloon is equivalent to maximizing the contained volume. The volume is given by $V = 4\pi \int_0^a r f(r) dr$, where $f(r)$ is the gross shape in the first quadrant, and a is the radius of the inflated shape. Because the material does not stretch a significant amount, the arclength of the curve $f(r)$ from 0 to a is fixed and equal to the radius of the original flat discs, W . Thus, the problem may be described by considering the volume of revolution defined by drawing a path of prescribed arclength $2W$ that starts and ends on the z -axis, sketched in Fig. 8a. The balloon shape is given by the path that maximizes this volume. The solution is an elliptic integral:

$$f(r) = \int_r^a \frac{s^2}{\sqrt{a^4 - s^4}} ds \quad 6.$$

for $0 \leq r \leq a$, where $a = 4W\sqrt{2\pi}/\Gamma(1/4)^2$. Figure 8b shows the shape for $W = 1$. Notably, the same shape describes the axisymmetric partial wrapping of a ultrathin sheet on a liquid droplet, shown in Fig. 7d, as well as the profile of the shortest possible axisymmetric dome that is supported only by internal pressure and meets the ground at right angles. This design was used for the Namihaya Dome in Osaka, Japan.

Computing the shape of an idealized circular mylar balloon is made tractable by virtue of an approximate axial symmetry. Extending this analysis to find the inflated shapes of other objects is a considerably more complex problem, although a general set of partial differential equations governing the final shape is known (100). Making headway on this problem is more than just an academic exercise — inflated membranes find use in a wide range of engineering applications (101, 102), such as the antenna shown in Fig. 8c.

6.2. Inflating polyhedral surfaces

Are there other general lessons that may be learned from inflating simple shapes? Suppose you assemble six squares of mylar into a cubical balloon that is flat on each face. Can you add more air to the balloon, without stretching it? Pak (103) provides a simple construction showing that the answer is yes. By bending material near the edges and corners to form new faces, the volume increases by 18.2%. (An earlier construction by Bleecker (104) gives

a 21.9% increase in volume; Buchin & Schulz (105) show how to obtain a 25.7% increase in volume.) Pak (106) proved that all polyhedral surfaces in \mathbb{R}^3 have volume-increasing isometric deformations, as originally conjectured by Bleecker (104).

What can we learn from a physical model? When a cubic balloon constructed from mylar panels is inflated, it forms wrinkles that are perpendicular to the 12 edges of the original cube. This response reveals something remarkable: material points are drawn towards each other in three-dimensional space as the volume increases. Thus, reducing the surface area of the *gross shape* can actually increase its capacity.

6.3. Parachutes and lobed balloons

The same principles that control the shape of a closed inflated membrane are at play in a deployed parachute. In the early 20th century, the Advisory Committee for Aeronautics in the United Kingdom was considering the design of parachutes. G. I. Taylor argued that if lightness is the primary goal, the parachute should be as flat as possible without forming wrinkles, since these features show there is extra material (107). The question then becomes: what is the flattest shape that will not form wrinkles when it is deployed?

To make headway, Taylor considered a disc of fabric containing many inextensible wires running from the center of the sheet. Air pressure pushes on the sheet; a cross section of the fabric between two wires is drawn in Fig. 9a. Force balance in the plane of the drawing shows that the fabric carries a lateral tension T given by:

$$2T \sin \theta = P\ell, \tag{7}$$

where P is the pressure difference across the membrane and θ is the angle the fabric makes with an imaginary line of length ℓ joining adjacent wires. If the number of wires is sufficiently large, the angle θ is independent of the number of wires (analogous to the slaving condition for sinusoidal wrinkles, Eq. 1). In the limit of infinitely many wires, the tension T

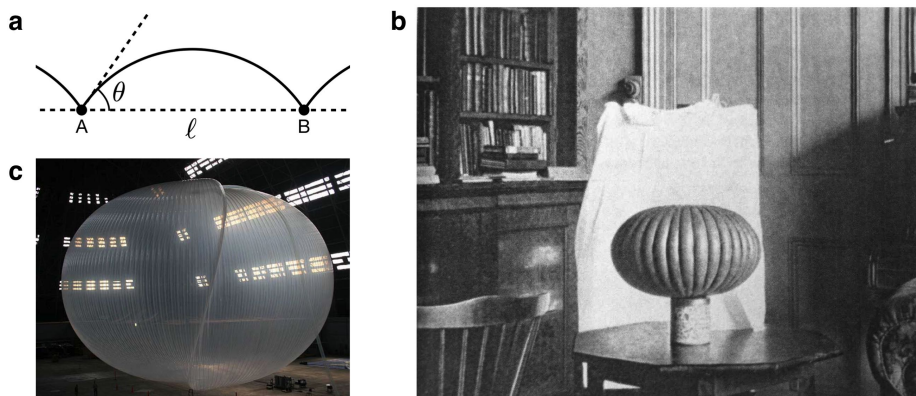


Figure 9

Circular parachutes and pumpkin balloons. (a) Cross section of a small portion of a parachute made from a disc of fabric with many radial wires, considered by G. I. Taylor (107). The fabric bulges out in a circular arc between two adjacent wires that run through the page at points A and B, a distance ℓ apart. (b) Model constructed by Taylor to test his predicted axisymmetric parachute shape (107). (c) Pumpkin balloon exhibiting an “s-cleft” instability (courtesy NASA).

vanishes (since in this case $\ell \rightarrow 0$, while P and θ are fixed). The deployed shape therefore carries stresses only along lines of longitude. Taking a further assumption that the pressure difference is constant over the membrane, the exact axisymmetric parachute shape may be determined using force balance on a small patch. The solution is the same elliptic integral of Eq. 6. Thus, the lightest possible axisymmetric parachute is formed by sewing panels together to form this gross shape, thereby avoiding the formation of wrinkles.

To test his predictions, Taylor built a simple tabletop model by attaching threads to a rubber balloon so that it could not stretch along lines of longitude. Comparing Taylor’s photograph in Fig. 9b to the mathematical curve in Fig. 8b, one can see that the reinforced balloon inflates to the same qualitative shape.

Radial threads are not required to form this profile — a parachute made from a stiff isotropic material deploys to the same gross shape. Nevertheless, the lobes in Taylor’s model are an ancestor to a balloon design developed by NASA in the 1990s (108). A so-called “pumpkin balloon” is made of high-strength wires spanned by a polymer sheet, which is overfilled with helium so that it remains at constant volume through temperature variations. This design subjects the envelope to relatively small stresses, so the sheet can be very thin ($\sim 10 \mu\text{m}$, similar to sandwich wrap) and lightweight, allowing for heavier payloads (109).

Unfortunately, there are unexpected limitations to this strategy: pumpkin balloons with many lobes are unstable to at least two types of buckling modes (see Reference 108 for a review). In the first type, the balloon is found to adopt a non-axisymmetric gross shape above a threshold pressure (110). In contrast to the purely geometric problems already discussed, this deformation requires finite stretching of the material. In the second type of buckling, a single s-shaped cleft appears, spanning the entire height of the balloon and several lobes in width, as shown in Fig. 9c. The clefted configuration is thought to be a local minimum of the total energy (111).

Numerical methods have been developed for studying the shape and stability of arbitrary inflated surfaces (112, 113). There is also an important and challenging inverse problem: going from a desired three-dimensional surface to a design for flat panels that may be sewn together and inflated into that shape. Recent progress has been made in developing computer algorithms for designing flat panels that inflate to a targeted shape (40).

7. CONCLUSION

The research reviewed here has considered the response of a wrapper and its contents to their mutual interaction. We paid special attention to two recent developments: a new class of so-called “asymptotic isometries” (60, 61, 63) and a geometric model for highly bendable sheets bound to liquid interfaces (86, 94). These advances are already bearing fruit: the geometric model separates geometry from mechanics, making a class of highly nonlinear problems tractable. At the same time, this model raises further questions about the relationship between microscopic buckled features and the gross shape of a deformed sheet. Some gross shapes are compatible with multiple possible microstructures (e.g., wrinkles, folds, crumples), whereas others seem to require a given feature, such as a fold (94).

There are also important unsolved problems that involve mechanics and materials. Thin sheets are prone to localize material into singular vertices and ridges, like the sharp corners in a crumpled piece of paper (114). Recent experiments found that the formation of smooth wrinkles and stress-focusing “crumples” are distinct symmetry-breaking events (56). The transition to the crumpled state, and the morphology and mechanics of the crumples, are

still not understood. What is the balance of forces that creates these features? Do they solve a mechanical problem, or a geometrical one? Other buckling motifs, such as the s-cleft in pumpkin balloons, await a fundamental understanding as well (111).

There are many extensions of the problems considered here. Thermal energies can become important for molecularly-thin materials such as graphene (115, 116, 117). The field of the statistical mechanics of thermalized ribbons and sheets is just in its infancy. Another class of problems involves stiffer sheets that are designed to hold their own shape, such as the capillary folding of hinged plates (118) and self-folding stimuli-responsive origami (119). Progress in this area may lead to microscopic machines and sensors that could interact with individual biological cells (120, 121).

As our physical understanding of thin films continues to develop, one large opportunity is in deploying thin films on liquid interfaces to perform tasks that are usually reserved for surfactants. Oil-water interfaces have been manipulated with soap for thousands of years and with particles for the last 100 years (96, 97, 98), and pre-fabricated capsules are used in a host of applications in foods, cosmetics, drugs, and agriculture (122). Thin, flexible sheets offer a paradigm for tailoring the physical and chemical properties of liquid surfaces in new ways (86, 95). Planar sheets can be prefabricated and dispersed in a continuous oil or water phase where they may self-attach to droplets. As we have seen, thin sheets automatically make optimally efficient droplet wrappers (86). Recent experiments have shown that a droplet impinging on a floating film can wrap itself using the fast dynamics of the impact, creating oil-in-water and water-in-oil wrappings with near-perfect seams (95). These results suggest a bright future for this new approach to an age-old problem.

DISCLOSURE STATEMENT

The author is not aware of any affiliations, memberships, funding, or financial holdings that might be perceived as affecting the objectivity of this review.

ACKNOWLEDGMENTS

I am grateful to Benny Davidovitch, Vincent Démery, Narayanan Menon, Sidney Nagel, Yousra Timounay, and Dominic Vella. I thank the Aspen Center for Physics for hospitality during early stages of this writing. Funding support from NSF-DMR-CAREER-1654102 is gratefully acknowledged.

LITERATURE CITED

1. Demaine ED, Demaine ML, Iacono J, Langerman S. 2009. *Computational geometry* 42:748–757
2. Chen Y, Guo F, Jachak A, Kim SP, Datta D, et al. 2012. *Nano Letters* 12:1996–2002
3. Py C, Reverdy P, Doppler L, Bico J, Roman B, Baroud C. 2007. *Physics of Fluids* 19:–
4. Audoly B, Pomeau Y. 2010. *Elasticity and geometry: from hair curls to the non-linear response of shells*. Oxford University Press
5. Vishtal A, Retulainen E. 2014. *BioResources* 9:7951–8001
6. Landau LD, Lifshitz E. 1986. *Course of Theoretical Physics* 3:109
7. Feynman RP, Leighton RB, Sands M. 1964. *Feynman lectures on physics*. vol. 2. Addison-Wesley
8. Pocivavsek L, Dellsy R, Kern A, Johnson S, Lin B, et al. 2008. *Science* 320:912–916

9. Diamant H, Witten TA. 2011. *Phys. Rev. Lett.* 107:164302
10. Brau F, Damman P, Diamant H, Witten TA. 2013. *Soft Matter* 9:8177–8186
11. Davidovitch B, Schroll RD, Cerda E. 2012. *Phys. Rev. E* 85:066115
12. Huang J, Davidovitch B, Santangelo CD, Russell TP, Menon N. 2010. *Phys. Rev. Lett.* 105:038302
13. Bowden N, Brittain S, Evans AG, Hutchinson JW, Whitesides GM. 1998. *Nature* 393:146–149
14. Brau F, Vandeparre H, Sabbah A, Poulard C, Boudaoud A, Damman P. 2011. *Nat Phys* 7:56–60
15. Cerda E, Mahadevan L. 2003. *Phys. Rev. Lett.* 90:074302
16. Paulsen JD, Hohlfeld E, King H, Huang J, Qiu Z, et al. 2016. *Proceedings of the National Academy of Sciences* 113:1144–1149
17. Taffetani M, Vella D. 2017. *Phil. Trans. R. Soc. A* 375:20160330
18. Huang J, Juszkiwicz M, de Jeu WH, Cerda E, Emrick T, et al. 2007. *Science* 317:650–653
19. Chung JY, Nolte AJ, Stafford CM. 2011. *Advanced materials* 23:349–368
20. Efimenko K, Rackaitis M, Manias E, Vaziri A, Mahadevan L, Genzer J. 2005. *Nature materials* 4:293–297
21. Chung JY, Youngblood JP, Stafford CM. 2007. *Soft Matter* 3:1163–1169
22. Chan EP, Smith EJ, Hayward RC, Crosby AJ. 2008. *Advanced Materials* 20:711–716
23. Zang J, Ryu S, Pugno N, Wang Q, Tu Q, et al. 2013. *Nature materials* 12:321–325
24. Levien R. 2008. *University of California, Berkeley, Technical Report No. UCB/EECS-2008-103*
25. Giomi L, Mahadevan L. 2012. *Proc. R. Soc. A* 468:1851–1864
26. Romero V, Witten T, Cerda E. 2008. *Proceedings of the Royal Society of London A: Mathematical, Physical and Engineering Sciences* 464:2847–2866
27. Audoly B. 2011. *Phys. Rev. E* 84:011605
28. Démery V, Davidovitch B, Santangelo CD. 2014. *Phys. Rev. E* 90:042401
29. Oshri O, Brau F, Diamant H. 2015. *Physical Review E* 91:052408
30. Sharon E, Roman B, Marder M, Shin GS, Swinney HL. 2002. *Nature* 419:579–579
31. Py C, Reverdy P, Doppler L, Bico J, Roman B, Baroud CN. 2007. *Phys. Rev. Lett.* 98:156103
32. Struik DJ. 2012. *Lectures on classical differential geometry*. Courier Corporation
33. Bico J, Roman B, Moulin L, Boudaoud A. 2004. *Nature* 432:690–690
34. Paretkar D, Xu X, Hui CY, Jagota A. 2014. *Soft Matter* 10:4084–4090
35. Mora S, Pomeau Y. 2015. *Journal of Physics: Condensed Matter* 27:194112
36. Style RW, Jagota A, Hui CY, Dufresne ER. 2017. *Annual Review of Condensed Matter Physics* 8:99–118
37. Bico J, Reyssat É, Roman B. 2017. *Annual Review of Fluid Mechanics* 50
38. Pokroy B, Kang SH, Mahadevan L, Aizenberg J. 2009. *Science* 323:237–240
39. Reis PM, Hure J, Jung S, Bush JWM, Clanet C. 2010. *Soft Matter* 6:5705–5708
40. Skouras M, Thomaszewski B, Kaufmann P, Garg A, Bickel B, et al. 2014. *ACM Transactions on Graphics (TOG)* 33:63
41. Guo X, Li H, Yeop Ahn B, Duoss EB, Hsia KJ, et al. 2009. *Proceedings of the National Academy of Sciences* 106:20149–20154
42. Jung S, Reis PM, James J, Clanet C, Bush JWM. 2009. *Physics of Fluids* 21:091110
43. Pogorelov AV. 1973. *Extrinsic geometry of convex surfaces*. vol. 35. American Mathematical Soc.
44. Ghys E. 2014. *Images of Mathematics, CNRS (images.math.cnrs.fr/Le-Brazuca-le-ballon-cubique-de-la-Coupe-du-monde)*
45. Hong S, Asai T. 2014. *Scientific reports* 4:5068
46. Hure J, Roman B, Bico J. 2011. *Phys. Rev. Lett.* 106:174301
47. Hure J, Roman B, Bico J. 2012. *Phys. Rev. Lett.* 109:054302
48. Majidi C, Adams GG. 2009. A simplified formulation of adhesion problems with elastic plates.

- In *Proceedings of the Royal Society of London A: Mathematical, Physical and Engineering Sciences*, vol. 465. The Royal Society
49. Hure J, Audoly B. 2013. *Journal of the Mechanics and Physics of Solids* 61:450–471
 50. Marchand A, Das S, Snoeijer JH, Andreotti B. 2012. *Physical review letters* 108:094301
 51. Nadermann N, Hui CY, Jagota A. 2013. *Proceedings of the National Academy of Sciences* 110:10541–10545
 52. Schulman RD, Dalnoki-Veress K. 2015. *Physical review letters* 115:206101
 53. Duprat C, Protiere S. 2015. *EPL (Europhysics Letters)* 111:56006
 54. Grason GM, Davidovitch B. 2013. *Proceedings of the National Academy of Sciences* 110:12893–12898
 55. Roman B, Pocheau A. 2012. *Physical review letters* 108:074301
 56. King H, Schroll RD, Davidovitch B, Menon N. 2012. *Proceedings of the National Academy of Sciences* 109:9716–9720
 57. Yao Z, Bowick M, Ma X, Sknepnek R. 2013. *EPL (Europhysics Letters)* 101:44007
 58. Aharoni H, Todorova DV, Albarrán O, Goehring L, Kamien RD, Katifori E. 2017. *Nature Communications* 8:15809
 59. Bella P, Kohn RV. 2017. *Phil. Trans. R. Soc. A* 375:20160157
 60. Hohlfeld E, Davidovitch B. 2015. *Phys. Rev. E* 91:012407
 61. Vella D, Huang J, Menon N, Russell TP, Davidovitch B. 2015. *Phys. Rev. Lett.* 114:014301
 62. Chopin J, Démery V, Davidovitch B. 2015. *Journal of Elasticity* 119:137–189
 63. Vella D, Ebrahimi H, Vaziri A, Davidovitch B. 2015. *EPL (Europhysics Letters)* 112:24007
 64. Lee C, Wei X, Kysar JW, Hone J. 2008. *science* 321:385–388
 65. Pharr GM, Herbert EG, Gao Y. 2010. *Annual Review of Materials Research* 40:271–292
 66. Roos W, Bruinsma R, Wuite G. 2010. *Nature physics* 6:733
 67. Gordon VD, Chen X, Hutchinson JW, Bausch AR, Marquez M, Weitz DA. 2004. *Journal of the American Chemical Society* 126:14117–14122
 68. Vella D, Ajdari A, Vaziri A, Boudaoud A. 2012. *Physical review letters* 109:144302
 69. Lazarus A, Florijn H, Reis PM. 2012. *Physical review letters* 109:144301
 70. Vella D, Ajdari A, Vaziri A, Boudaoud A. 2011. *Phys. Rev. Lett.* 107:174301
 71. Vella D, Davidovitch B. 2018. *arXiv:1804.03341*
 72. Holmes DP, Crosby AJ. 2010. *Phys. Rev. Lett.* 105:038303
 73. Ripp MM, Démery V, Zhang T, Paulsen JD. 2018. *arXiv:1804.02421*
 74. Gomez M, Moulton DE, Vella D. 2016. *Proc. R. Soc. A* 472:20150732
 75. Vaziri A, Mahadevan L. 2008. *Proceedings of the National Academy of Sciences* 105:7913–7918
 76. Nasto A, Ajdari A, Lazarus A, Vaziri A, Reis PM. 2013. *Soft Matter* 9:6796–6803
 77. Green AE. 1937. The elastic stability of a thin twisted strip—ii. In *Proc. R. Soc. Lond. A*, vol. 161. The Royal Society
 78. Chopin J, Kudrolli A. 2013. *Phys. Rev. Lett.* 111:174302
 79. Korte A, Starostin E, Van Der Heijden G. 2010. Triangular buckling patterns of twisted inextensible strips. In *Proceedings of the Royal Society of London A: Mathematical, Physical and Engineering Sciences*. The Royal Society
 80. Dinh HP, Démery V, Davidovitch B, Brau F, Damman P. 2016. *Physical review letters* 117:104301
 81. Audoly B, Boudaoud A. 2003. *Physical review letters* 91:086105
 82. Giomi L, Mahadevan L. 2010. *Physical review letters* 104:238104
 83. Klein Y, Venkataramani S, Sharon E. 2011. *Physical review letters* 106:118303
 84. Gemmer J, Venkataramani S. 2012. *Nonlinearity* 25:3553
 85. Dias MA, Dudte LH, Mahadevan L, Santangelo CD. 2012. *Physical review letters* 109:114301
 86. Paulsen JD, Démery V, Santangelo CD, Russell TP, Davidovitch B, Menon N. 2015. *Nature materials* 14:1206–1209
 87. Brakke KA. 1992. *Experimental Mathematics* 1:141–165

88. Gao L, McCarthy TJ. 2008. *Langmuir* 24:9183–9188
89. Milner ST, Joanny JF, Pincus P. 1989. *EPL (Europhysics Letters)* 9:495
90. Hunt GW, Wade MK, Shiacolas N. 1993. *Journal of applied mechanics* 60:1033
91. Reis PM, Corson F, Boudaoud A, Roman B. 2009. *Physical review letters* 103:045501
92. Leahy BD, Pocivavsek L, Meron M, Lam KL, Salas D, et al. 2010. *Physical review letters* 105:058301
93. Pineirua M, Tanaka N, Roman B, Bico J. 2013. *Soft Matter* 9:10985–10992
94. Paulsen JD, Démary V, Toga KB, Qiu Z, Russell TP, et al. 2017. *Physical Review Letters* 118:048004
95. Kumar D, Paulsen JD, Russell TP, Menon N. 2018. *Science* 359:775–778
96. Binks BP. 2002. *Current Opinion in Colloid & Interface Science* 7:21–41
97. Subramaniam AB, Abkarian M, Mahadevan L, Stone HA. 2005. *Nature* 438:930–930
98. Cui M, Emrick T, Russell TP. 2013. *Science* 342:460–463
99. Paulsen WH. 1994. *The American Mathematical Monthly* 101:953–958
100. Deakin MA. 2009. *Bulletin of the Australian Mathematical Society* 80:506–509
101. Salama M, Lou M, Fang H. 2000. Deployment of inflatable space structures: A review of recent developments. Tech. rep., AIAA-2000-1730
102. Mladenov IM, Oprea J, et al. 2009. *J. Geom. Symm. Phys* 15:53–88
103. Pak I. 2008. *The American Mathematical Monthly* 115:443–445
104. Bleecker DD, et al. 1996. *Journal of Differential Geometry* 43:505–526
105. Buchin K, Schulz A. 2007. Inflating the cube by shrinking. In *Proceedings of the twenty-third annual symposium on Computational geometry*. ACM
106. Pak I. 2006. Preprint, Department of Mathematics, MIT
107. Taylor GI. 1963. On the shapes of parachutes (paper written for the Advisory Committee for Aeronautics, 1919) in the scientific papers of Sir Geoffrey Ingram Taylor. vol. 3. Cambridge Univ. Press
108. Pagitz M. 2007. *Philosophical Transactions of the Royal Society of London A: Mathematical, Physical and Engineering Sciences* 365:3003–3017
109. Lennon A, Pellegrino S. 2005. Structural mechanics of lobed inflatable structures. In *Spacecraft Structures, Materials and Mechanical Testing 2005*, vol. 581
110. Pagitz M, Pellegrino S. 2010. *International Journal of Solids and Structures* 47:1496–1507
111. Deng X, Pellegrino S. 2011. A technique to predict clefting of lobed super-pressure balloons. In *11th AIAA Aviation Technology, Integration, and Operations (ATIO) Conference*
112. Barsotti R, Ligarò SS. 2014. *Computational Mechanics* 53:1001–1013
113. Vetter R, Stoop N, Wittel FK, Herrmann HJ. 2014. Simulating thin sheets: Buckling, wrinkling, folding and growth. In *Journal of Physics: Conference Series*, vol. 487. IOP Publishing
114. Witten TA. 2007. *Rev. Mod. Phys.* 79:643–675
115. Bles MK, Barnard AW, Rose PA, Roberts SP, McGill KL, et al. 2015. *Nature* 524:204
116. Košmrlj A, Nelson DR. 2016. *Physical Review B* 93:125431
117. Yllanes D, Bhabesh SS, Nelson DR, Bowick MJ. 2017. *Nature Communications* 8:1381
118. Shenoy VB, Gracias DH. 2012. *Mrs Bulletin* 37:847–854
119. Na JH, Evans AA, Bae J, Chiappelli MC, Santangelo CD, et al. 2015. *Advanced Materials* 27:79–85
120. Xu W, Qin Z, Chen CT, Kwag HR, Ma Q, et al. 2017. *Science advances* 3:e1701084
121. Miskin MZ, Dorsey KJ, Bircan B, Han Y, Muller DA, et al. 2018. *Proceedings of the National Academy of Sciences* 115:466–470
122. Amstad E. 2017. *ACS Macro Letters* 6:841–847